9-23-2011

Exploring The Roles of Nucleobase Desolvation and Shape Complementarity During The Misreplication of O6-Methylguanine

Delia Chavarria
Case Western Reserve University

Andrea Ramos Serrano
Case Western Reserve University

Ichiro Hirao
University of Michigan

Anthony J. Berdis
Cleveland State University, A.BERDIS@csuohio.edu

Exploring the Roles of Nucleobase Desolvation and Shape Complementarity during the Misreplication of O^6-Methylguanine

Delia Chavarria , **Andrea Ramos-Serrano** , **Ichiro Hirao** , and **Anthony J. Berdis**

Abstract

O^6-methylguanine is a miscoding DNA lesion arising from the alkylation of guanine. This report uses the bacteriophage T4 DNA polymerase as a model to probe the roles hydrogen-bonding interactions, shape/size, and nucleobase desolvation during the replication of this miscoding lesion. This was accomplished by using transient kinetic techniques to monitor the kinetic parameters for incorporating and extending natural and non-natural nucleotides. In general, the efficiency of nucleotide incorporation does not depend on the hydrogen-bonding potential of the incoming nucleotide. Instead, nucleobase hydrophobicity and shape complementarity appear to be the preeminent factors controlling nucleotide incorporation. In addition, shape complementarity plays a large role in controlling the extension of various mispairs containing O^6-methylguanine. This is evident as the rate constants for extension correlate with proper interglycosyl distances and symmetry between the base angles of the formed mispair. Base pairs not conforming to an acceptable geometry within the polymerase's active site are refractory to elongation and are processed via exonuclease proofreading. The collective data set encompassing nucleotide incorporation, extension, and excision is used to generate a model accounting for the mutagenic potential of O^6-methylguanine observed *in vivo*. In addition, kinetic studies monitoring the incorporation and extension of non-natural nucleotides identified an analog that displays high selectivity for incorporation opposite O^6-methylguanine compared to unmodified purines. The unusual selectivity of this analog for replicating damaged DNA provides a novel biochemical tool to study translesion DNA synthesis.

Keywords

DNA replication; mutagenesis; polymerase fidelity; desolvation; non-natural nucleotides

Introduction

Most models accounting for efficient and faithful DNA polymerization invoke the importance of correct hydrogen-bonding interactions between an incoming nucleotide and its templating partner. The mutual recognition of adenine (A) by thymine (T) and of guanine (G) by cytosine (C) involves the ability of the DNA polymerase to consummate the formation of precise hydrogen-bonding interactions between each partner. In this model, specific pairing between hydrogen bonding groups provides high fidelity DNA polymerases with enough flexibility to recognize four distinct pairing partners (A:T, G:C, T:A, and C:G) while retaining enough stringency to maintain exquisite genomic fidelity. Indeed, replicative DNA polymerases display low error frequencies of ~1 mistake every 10^6 base pairs (1), and this high degree of fidelity has historically been attributed to the utilization of these hydrogen bonding interactions. Further support of this model has been inferred by significant changes in the efficiency and fidelity of polymerization when the chemical composition and hydrogen-bonding interactions of a templating nucleobase are modified (2–4). This is particularly evident with DNA lesions such as N^3-methyladenine (5), N^7-methylguanine (6), and O^6-methylguanine (7, 8) that are formed by anti-cancer agents such as temozolomide and BCNU. Although these lesions can be corrected by various DNA repair pathways (9–11), they sometimes escape repair and are misreplicated by DNA polymerases (12–15). O^6-methylguanine (O^6-MeG) is a particularly interesting lesion as the simple introduction of a methyl group results in a higher frequency of dTTP misincorporation events (12–15). If left unrepaired, the formed T:O^6-MeG mispair can be further replicated to yield C:G to T:A transition mutations that can spark the initiation of genetic diseases such as cancer.

The preferential insertion of dTMP opposite O^6-MeG is generally attributed to alterations to the hydrogen-bonding functional groups of guanine. Indeed, simple inspection of the structures provided in Figure 1A suggests that a T:O^6-MeG base-pair possesses more favorable hydrogen-bonding interactions compared to C:O^6-MeG. However, other biophysical features such as π–π stacking interactions, nucleobase hydrophobicity, and geometrical constraints are also likely to contribute to this process. Indeed, the addition of a methyl group to the O6 position of guanine produces a variety of effects including changes in nucleobase hydrophobicity, increasing the overall size and shape of the nucleobase, and changing its tautomeric form to influence π–π stacking interactions. As a consequence of these changes, the mechanism of nucleotide selection and incorporation opposite this DNA lesion may involve biophysical features that are distinct from simple hydrogen-bonding interactions.

This report examines the roles of hydrogen-bonding, shape complementarity, and nucleobase hydrophobicity during the misreplication of O^6-MeG by measuring the kinetics of incorporation, extension, and excision of a series of natural and non-natural nucleotides. We used the bacteriophage T4 DNA as a model since it replicates unmodified DNA with incredibly high fidelity (16–18). In addition, it is functionally homologous to eukaryotic DNA polymerases such as pol δ and pol ε that are involved in chromosomal replication (19). We demonstrate here that the kinetic parameters for nucleotide incorporation opposite the miscoding O^6-MeG lesion depend upon the base-stacking potential of the incoming nucleotide rather than hydrogen-bonding interactions. In contrast, extension beyond O^6-MeG is influenced primarily by two biophysical parameters, interglycosyl distance and base angles, that define shape complementarity of the formed mispair. Perturbations in either parameter activates exonuclease proofreading activity that subsequently removes mispairs and prevents the propagation of possible genomic errors. Our analyses show that the "correct" C:O^6-MeG pair is effectively excised while the incorrect T:O^6-MeG mispair escapes detection and is elongated rather than degraded. These results demonstrate that

unbalanced proofreading activity causes an overall kinetic flux favoring the stable incorporation of dTTP opposite O^6-MeG. The collective data set is used to propose a new model explaining the pro-mutagenic behavior of O^6-MeG.

Results

Kinetic Parameters for the Incorporation of dCMP and dTMP Opposite O^6-Methylguanine

DNA polymerases utilize the multi-step pathway illustrated in Figure 2 to achieve efficient and accurate DNA synthesis (20–23). These steps include nucleotide incorporation (Step A), elongation of the incorporated nucleotide (Step B), and exonuclease-proofreading that can excise any misincorporated nucleotide (Step C). Of these three steps, nucleotide incorporation is considered to be the most important control point for maintaining fidelity. This step is further composed of several distinct microscopic kinetic events that include dNTP binding to the polymerase nucleic acid complex, a conformational change step that further aligns the incoming dNTP into a correct geometrical arrangement with its templating partner, and the phosphoryl transfer step that covalently attaches the incoming nucleotide to the primer (Figure 2B). Collectively, these kinetic steps provide an error frequency of 1 misincorporation event per 10^5–10^6 turnovers during the replication of undamaged DNA (1).

To evaluate the contribution of these individual steps during translesion DNA synthesis, we measured kinetic dissociation constants (K_d)* and maximal polymerization rate constants (k_{pol}) for the incorporation of dCTP and dTTP opposite O^6-MeG using rapid quench chemical techniques (24). Data provided in Figure 3A illustrate how the kinetics of polymerization are influenced as a function of increasing dCTP concentrations.^ All time courses were fit to the equation for a single exponential process to define k_{obs}, the rate constant in product formation. The plot of k_{obs} versus dCTP concentration is hyperbolic (Figure 3B), and a fit of the data to the Michaelis-Menten equation (equation 2) yields a k_{pol} of 1.5 +/− 0.2 sec^{-1}, a K_d of 48 +/− 16 μM, and a k_{pol}/K_d of 31,250 +/− 9,500 $M^{-1}sec^{-1}$. Identical analyses performed using dTTP as the substrate yield a k_{pol} of 114 +/− 20 sec^{-1}, a K_d of 760 +/− 230 μM, and k_{pol}/K_d of 150,000 +/− 24,500 $M^{-1}sec^{-1}$ (Supplemental Figures 2). Values for k_{pol}, K_d, and k_{pol}/K_d are summarized in Table 1.

Similar experiments were performed to define the kinetic parameters for correctly incorporating dCTP opposite G (Supplemental Figure 3) as well as for the misincorporation of dATP and dTTP opposite G (Supplemental Figures 4A and 4B, respectively). Table 1 provides a summary of k_{pol}, K_d, and k_{pol}/K_d values for the correct and incorrect incorporation of natural nucleotides opposite O^6-MeG, G, and A. Inspection of the collective data set shows that the overall catalytic efficiency for replicating O^6-MeG is ~1,000-fold lower than that for replicating a correct C:G base pair. While this difference argues that the misreplication of O^6-MeG is rather inefficient, it should be noted that the catalytic efficiency for incorporating dTTP opposite O^6-MeG is ~100-fold higher than that for forming natural mispairs such as T:G. At face value, the higher efficiency for replicating O^6-MeG provides an explanation for its pro-mutagenic behavior. However, the experimental sections

*The measured values closely approximate a true dissociation constant (K_d) since reactions were performed using single turnover conditions and the rate limiting step for incorporation is likely to be the conformational change preceding phosphoryl transfer.
^Despite the use of single turnover reaction conditions, denaturing gel electrophoresis data reveals that only 50% of DNA containing O^6-MeG is elongated regardless of whether dCTP, dTTP, or mixtures of dCTP/dTTP are used (Supplemental Figure 1). However, the inability to obtain 100% substrate turnover does not impact of the interpretations of experiments performed using single turnover reaction conditions since the rate constant in product formation is unaffected by the presence of DNA that cannot be elongated. This condition is not met using pseudo-first order reaction conditions as the presence of a non-usable DNA substrate will generate lower initial velocity rates that can lead to erroneous K_m and/or k_{cat} values.

described below demonstrate that mispair elongation and exonuclease proofreading activity contribute more significantly to the pro-mutagenic properties of O^6-MeG.

Kinetic Parameters for Non-Natural Nucleotides Opposite O^6-Methylguanine

The incorporation of several non-natural pyrimidine analogs opposite O^6-MeG were also measured to further probe the roles of hydrogen bonding, shape complementarity, and nucleobase hydrophobicity during nucleotide selection. Initial attempts focused on P-nucleotide (((2R,3R,5R)-3-hydroxy-5-(7-oxo-7,8-dihydro-3H-pyrimido[4,5-c][1,2]oxazin-6(4H)-yl)tetrahydrofuran-2-yl)methyl triphosphate) (Figure 4A) as this non-natural nucleobase retains the same hydrogen-bonding functional groups of cytidine but is locked in a tautomeric form that resembles thymine. These biophysical features led us to predict that P-nucleotide would display a fast k_{pol} value like dTTP and a low K_d value like dCTP. As such, it is quite surprising that P-nucleotide is poorly incorporated opposite O^6-MeG (Figure 4B), displaying a low catalytic efficiency of $2*10^4$ $M^{-1}sec^{-1}$ that is caused primarily by poor binding affinity (K_d >500 μM).

The kinetic parameters for Zebularine (Figure 4A), a cytidine analog containing a 2-(1H)-pyrimidone ring, were next measured. Zebularine is also poorly incorporated opposite O^6-MeG, displaying a k_{pol}/K_d value of 170 +/− 50 $M^{-1}sec^{-1}$ (data not shown). In this case, the poor catalytic efficiency is caused by a high K_d value of 660 +/− 100 μM coupled with a low k_{pol} value of 0.11 +/− 0.03 sec^{-1}. The final non-natural nucleotide tested was 4-methyl-pyrimidone-2′-deoxynucleoside triphosphate (4-MePoTP) (Figure 4A). While 4-MePoTP is similar in shape and size to dCTP and dTTP, it is considerably more hydrophobic due to the substitution of a methyl group for the -NH_2 group of dCTP and the keto oxygen of dTTP. Although 4-MePoTP lacks two key hydrogen bonding groups, it is efficiently incorporated opposite O^6-MeG (Figure 4C). In fact, the k_{pol}/K_d value of 89,000 $M^{-1}sec^{-1}$ is ~3-fold higher than that measured for dCTP and only 1.7-fold lower than dTTP. The k_{pol} for 4-MePoTP is relatively fast at 18 sec^{-1} while the K_d value is ~200 μM. Although the K_d value of 200 μM is still high, it is significantly lower than values measured for nucleotides such as dTTP (700 μM), P-nucleotide (>500 μM), and Zebularine (660 μM) which contain hydrogen-bonding groups.

Elongation Beyond Properly Paired and Mispaired Primer/Templates

After incorporation opposite a DNA lesion, polymerases have the opportunity to extend beyond the formed mispair to propagate a potential genomic error (Figure 2A). Using the experimental protocol outlined in Figure 5A, we tested the ability of the exonuclease-deficient bacteriophage T4 DNA polymerase to extend beyond O^6-MeG. In these experiments, 1 μM gp43 exo was pre-incubated with 250 nM DNA containing O^6-MeG for 10 seconds and then supplied with 100 μM natural nucleotide (dCTP or dTTP) or 500 μM non-natural nucleotide (P-nucleotide, Zebularine, 4-MePoTP) for time intervals that allow for significant insertion opposite the lesion. After this time, 100 μM dGTP was added to initiate elongation beyond the lesion. Representative gel electrophoresis data provided in Figure 5B (left panel) shows that the exonuclease deficient T4 DNA polymerase (gp43 exo) effectively extends beyond all natural and non-natural mispairs formed with O^6-MeG.

To further quantify differences between correct and translesion DNA synthesis, we used rapid quench techniques to monitor extension reactions on short time intervals ranging from 0.005 to 5 seconds. DNA synthesis on an undamaged DNA template is highly efficient as the 13-mer is completely and rapidly elongated to the expected 17-mer (Figure 6A). Kinetic simulations were performed as previously described (25) on the time courses provided in Figure 6B to define rate constants for each extension step (k_{ext}). As expected for correct

DNA synthesis, the k_{ext} values for all elongation events on undamaged DNA are extremely fast, ranging from 50 to 200 sec^{-1}.

k_{ext} values for extending T:O^6-MeG or C:O^6-MeG were next measured to identify potential differences in propagating these potential mismatches. Time courses for elongation beyond a T:O^6-MeG mispair are provided in Figure 6C and were fit using the k_{ext} values listed in Table 2. It is noteworthy that extension beyond T:O^6MeG is remarkably efficient as the k_{ext} of ~50 sec^{-1} is only 2-fold slower than that measured for extending a correct C:G base pair. Similar analysis monitoring elongation beyond C:O^6-MeG (data not shown) yields a k_{ext} value of 2.5 sec^{-1} (Table 2). Thus, elongation of a C:O^6-MeG base pair is ~40-fold slower than that for extending beyond a correct C:G base pair and ~25-fold slower than extending beyond a T:O^6-MeG.

Rate constants for extending beyond T:G and A:G mispairs were also measured to compare the efficiency for misreplicating natural mispairs to those containing O^6-MeG. Extension beyond an A:G mispair is not observed even after a reaction time of 5 minutes. In contrast, a T:G mispair is extended far more efficiently as products corresponding to 17-mers are observed within 5 seconds(data not shown). The time courses in elongating a T:G mispair were best fit using the k_{ext} values reported in Table 2. It is particularly interesting to note that a T:G mispair is extended significantly slower than a T:O^6-MeG mispair (compare 2.7 sec^{-1} versus 50 sec^{-1}, respectively).

Similar experiments monitored the ability of wild-type T4 DNA polymerase (gp43 exo^+) to extend natural and non-natural mispairs containing O^6-MeG. Gel electrophoresis data provided in Figure 5B (right panel) shows that the proofreading capabilities are dependent upon the nature of the formed mispair. For example, gp43 exo^+ easily extends T:O^6-MeG mispair yet elongates the C:O^6-MeG mispair far less proficiently, even when supplied with high concentrations of dGTP (500 μM). The reduced efficiency for extending C:O^6-MeG is likely caused by rapid removal of dCMP which precludes dGTP incorporation at the next correct templating position. Similar results are observed when P-nucleotide and Zebularine paired opposite O^6-MeG. Close inspection reveals that gp43 exo^+ extends beyond P-nucleotide with an efficiency similar to dCTP while Zebularine is not extended at all. It should be emphasized that the degradation of P-nucleotide is not caused by introducing additional bulk to the nucleobase since P-nucleotide is efficiently elongated when paired opposite guanine (Supplemental Figure 5). However, the most surprising result is the ability of gp43 exo^+ to extend beyond 4-MePoTP where paired opposite O^6-MeG. In fact, 4-MePoTP is extended as effectively as T. This result provides the first evidence for the facile replication of a non-natural base pair even in the presence of vigorous exonuclease proofreading.

Discussion

O^6-methylguanine is a promiscuous and highly pro-mutagenic DNA lesion as dTTP is typically incorporated more efficiently that the “correct” nucleotide, dCTP. Attempts to reconcile this promiscuous behavior have primarily focused on correlating the kinetic parameters of nucleotide incorporation with perturbations in hydrogen bonding interactions. The preferential incorporation of dTTP is argued to reflect more favorable hydrogen bonding patterns made between the T:O^6-MeG mispair compared to that for C:O^6-MeG (Figure 1A). Indeed, our data obtained with the high fidelity bacteriophage T4 DNA polymerase also illustrates that dTTP is utilized with a 5-fold higher catalytic efficiency than dCTP. Similar results have been reported with other high-fidelity DNA polymerases including the bacteriophage T7 polymerase (26) and the eukaryotic polymerases, pol δ (27,

28). In each case, dTTP is incorporated opposite O^6-MeG with similar or higher catalytic efficiencies than dCTP.

While the 5-fold difference measured here with the bacteriophage T4 polymerase could reflect alterations in hydrogen bonding interactions, there are several notable dichotomies in the kinetic parameters that argue against this simple mechanism. For example, the extremely high K_d of 760 μM for dTTP is not consistent with more stable hydrogen bonding interactions with O^6-MeG. Likewise, the lower K_d value of 48 μM for dCTP also contradicts a model invoking direct hydrogen bonding interactions as the C:O^6-MeG mispair is predicted to be less thermodynamically stable. Another interesting dichotomy is the disparity in k_{pol} values measured with dTTP and dCTP. Despite the extremely high K_d value for dTTP, it is incorporated opposite O^6-MeG with a fast k_{pol} value of 114 sec^{-1} that rivals the k_{pol} of 100 sec^{-1} measured for inserting dTTP opposite adenine (29). Although dCTP binds with higher affinity, the measured k_{pol} of 1.5 sec^{-1} is significantly slower than that of 114 sec^{-1} measured using dTTP. Collectively, the differences in the K_d values indicate that dNTP binding, at least with the high-fidelity bacteriophage T4 DNA polymerase, is not directly governed by hydrogen bonding interactions. However, it is possible that k_{pol} values are more sensitive to proper hydrogen bonding contacts made during the conformational change step that precedes phosphoryl transfer. In particular, the faster k_{pol} of 114 sec^{-1} measured with dTTP could reflect optimal hydrogen bonding interactions that facilitate a rate-limiting conformational change step (30, 31) whereas the slower k_{pol} value could reflect non-optimal hydrogen-bonding interactions between dCTP and O^6-MeG that reduces the rate of this kinetic step.

The role of hydrogen bonding interactions was interrogated further by measuring K_d and k_{pol} values for non-natural nucleotides opposite O^6-MeG and undamaged purines. The kinetic parameters summarized in Table 1 indicate that while hydrogen bonding interactions are important for correct DNA synthesis, there are dispensable for efficient translesion DNA synthesis. This is perhaps best illustrated by examining the utilization of P-nucleotide, a pyrimidine analog that has the same hydrogen-bonding functional groups of cytidine but that is locked in a tautomeric form resembling thymine. These features allow P-nucleotide to be incorporated opposite either G or A with high catalytic efficiencies approaching 10^6 $M^{-1}sec^{-1}$. However, P-nucleotide is incorporated poorly opposite O^6-MeG despite the fact that it possesses the same tautomeric form and hydrogen-bonding capabilities as dTTP. In fact, the catalytic efficiency for incorporating P-nucleotide opposite O^6-MeG is ~7-fold lower than that measured for dTTP. Similar results are obtained with Zebularine, an analog resembling dCTP, as it is also a poor nucleotide substrate for O^6-MeG. In this case, the k_{pol}/K_d for Zebularine is ~100-fold lower than dCTP. In general, the poor catalytic efficiency for either non-natural nucleotide suggests that efficient incorporation does not correlate with the capacity to form favorable hydrogen bonds with O^6-MeG.

This argument is strengthened by the observation that 4-MePoTP, an pyrimidine analog that lacks key hydrogen bonding groups, is incorporated opposite O^6-MeG with a surprisingly high catalytic efficiency of 89,000 $M^{-1}sec^{-1}$. In this case, the increase in nucleobase hydrophobicity coupled with adequate shape complementarity between 4-MePoTP and O^6-MeG generates favorable conditions for nucleotide binding and incorporation. This argument makes intuitive sense as alkylation of guanine makes the templating base more hydrophobic. Indeed, “hydrophobic” nucleotides such as dTTP and 4-MePoTP are incorporated with higher catalytic efficiencies compared to more “hydrophilic” nucleotides such as dCTP, P-nucleotide, and Zebularine. This conclusion is consistent with reports indicating that interactions between two hydrophobic nucleobases are stronger than those made between mixed base pairs, i.e., a hydrophobic base paired with a hydrophilic base (32–35). This mechanism is further corroborated by the results presented here demonstrating that

the hydrophobic nucleotide, 4-MePoTP, is poorly incorporated opposite either a templating G or A due to unfavorable enthalpic interactions of a hydrophobic nucleobase with one that is hydrophilic. Likewise, P-nucleotide, which is relatively hydrophilic, is poorly incorporated opposite the hydrophobic miscoding lesion but efficiently incorporated opposite natural purines.

While these results highlight the consequences of nucleobase modification on polymerization fidelity, they also have practical applications. In particular, the results here demonstrate that 4-MePoTP is 100-fold more selective for incorporation opposite O^6-MeG than natural nucleobases such as A or G (Figure 7). The unusual selectivity of 4-MePoTP for this lesion suggests that it could be used as a reagent in PCR to selectively amplify DNA containing O^6-MeG. This is possible since the non-natural nucleotide is efficiently elongated when paired opposite the miscoding lesion, even in the presence of vigorous exonuclease proofreading capabilities. In addition, this non-natural nucleotide could be used as a chemical tool to specifically monitor the misreplication of O^6-MeG that exists in genomic DNA. We are actively exploring these potential research areas to generate novel tools for synthetic biology.

Mispair Extension is Influenced by Shape Complementarity

While the catalytic efficiencies for incorporating dTTP versus dCTP opposite O^6-MeG differ, more significant variations exist in the efficiency for elongating either mispair. Specifically, extension beyond T:O^6-MeG is 20-fold faster compared to C:O^6-MeG (k_{ext} of 50 sec^{-1} versus 2.5 sec^{-1}, respectively). These kinetic differences are likely caused by perturbations in overall shape complementarity of the formed mispair, a model originally proposed by Kool and colleagues to account for replication in the absence of hydrogen-bonding interactions (36, 37). For extension kinetics, we attribute shape complementarity to reflect optimal interglycosyl distances (length between the C1′ of either ribosyl group in the base pair) coupled with symmetrical base angles (angle between the C1 of ribose with the N9 of a purine or N1 of pyrimidine). As summarized in Table 3, values that correspond to interglycosyl distance and bond angles vary significantly between correct and mismatched base pairs. For example, proper A:T and G:C base pairs have an interglycosyl distance of ~10.4Å and symmetrical base angles of ~55°. These parameters define the optimal geometry of a typical Watson-Crick base pair which are consistent with fast k_{ext} values of 100 sec^{-1}. It is clear that mispairs that have changes in bond angle and/or interglycosyl distance have reduced k_{ext} values. However, a closer inspection of the data reveals that perturbations in the size of the mispair may play a more significant role in hindering mispair elongation compared to alterations in nucleobase angles. This is evident as a purine:purine mismatch (A:G), which possesses a larger interglycosyl distance of 12.5Å, is not elongated while a pyrimidine:purine mismatch (T:G) that has a smaller interglycosyl distance of 10.4Å is elongated despite having asymmetric perturbations in nucleobase angles of 42° and 70°, respectively. Based upon this analysis, it is not surprising that T:O^6-MeG is efficiently extended (k_{ext} = 50 sec^{-1}) as the interglycosyl distance of 10.5Å and nucleobase angles of ~53° resemble the parameters for a natural base pair. In contrast, the C:O^6-MeG base pair shows significant perturbations in bond angles (asymmetry of 66° and 43°) and interglycosyl distance (11.4Å), and these perturbations coincide with a lower k_{ext} of 2.5 sec^{-1}. The importance of these features on pro-mutagenic synthesis is discussed further within the context of exonuclease proofreading (vide infra). However, one interesting exception to this characterization is the facile elongation of 4-MePo when paired opposite O^6-MeG. In this case, extension beyond this mispair should not occur since the interglycosyl distance of 10.8Å is larger than 10.4Å for a correct base pair. This dichotomy could reflect inherent limitations in the software used to calculate interglycosyl distances as enthalpic contributions mediated by hydrogen-bonding interactions are weighted heavily in these

calculations. An alternative possibility is that this non-natural base pair is flexible and can adopt different conformations that allow for subsequent elongation. This explanation is based upon recent structural studies of the thermostable *Bacillus*DNA polymerase I during the replication and extension of this miscoding nucleobase (15). These studies reveal that O^6-MeG in the template can adopt distinct configurations that are essential for efficient elongation. When the polymerase is bound with a template O^6-MeG paired opposite an incoming ddTTP or ddCTP, the methyl group of the miscoding lesion is pointed toward the Watson–Crick face and is interposed between the O-6 group of guanine and the carbonyl oxygen (O-4) of thymine or the amine group of cytosine. Although this result conflicts with published NMR studies (38), it is consistent with X-ray structures of DNA alone indicating that the methyl group of O^6-MeG is oriented in the *syn* configuration and pointed towards the templating nucleobase (39). Regardless, the structures of polymerase:DNA complexes reveal that both base pairs containing O^6-MeG adopt a conformation that is nearly identical to a correct C:G base pair, the key exception being that the lesion is slightly twisted out of plane(15). However, more important differences are observed in the structures of the polymerase bound to either elongated mispair (15). In these structures, the methyl group of O^6-MeG is still pointed toward the thymine carbonyl of the extended T:O^6-MeG mispair. However, a change from B- to A-form DNA occurs upon binding of the polymerase and generates enough space for the methyl group to form weak yet favorable interactions with the carbonyl oxygen of thymine. In contrast, the position of the methyl group is not defined in the C:O^6-MeG pair, suggesting that it can adopt both *syn*- and *anti*-configurations. The difference in methyl group orientation provides a reasonable molecular explanation as to why C:O^6-MeG is degraded while C:O^6-MeG and 4-MePo:O^6-MeG are elongated even in the presence of exonuclease proofreading. Additional studies are needed to evaluate the structural features of DNA containing 4-MePo paired opposite O^6-MeG to further interrogate this mechanism.

Lapses in Exonuclease Proofreading Enhance Pro-Mutagenic DNA Synthesis

The pro-mutagenic potential of O^6-MeG is often attributed to defects in polymerization fidelity (12–15). We argue that the 5-fold higher catalytic efficiency for incorporating dTTP is not enough to entirely account for the pro-mutagenic behavior of this miscoding DNA lesion. Instead, a more significant effect is caused by the preferential elongation of T:O^6-MeG mispair compared to the “correct” C:O^6-MeG. It is indeed striking that the wild-type DNA polymerase efficiently extends the pro-mutagenic T:O^6-MeG base pair while it rapidly degrades the correct C:O^6-MeG pair. The decision to extend rather than degrade the mispair appears intimately linked with perturbations in the interglycosyl distance and/or base angles of the formed mispair. As before, the T:O^6-MeG mispair is elongated since these parameters closely mimic a correct C:G base pair whereas the correct C:O^6-MeG pair is degraded as these parameters are significantly perturbed. This information has a significant impact on genomic fidelity as unbalanced proofreading activity generates an overall net flux that favors the stable incorporation of dTTP opposite O^6-MeG. In the mechanism outlined in Figure 8, defects in nucleotide excision amplify the minimal effects caused by the preferential incorporation of dTTP. This predicts that the T:O^6-MeG pair would misreplicated during the next round of replication to generate a T:A pair in one DNA strand while the T:O^6-MeG mispair would be regenerated on the other.

It is interesting that replication of O^6-MeG by high-fidelity polymerases is error-prone and contrasts the activity of specialized DNA polymerases such as Dpo4 (40) and eukaryotic DNA polymerases including pol η (41) and Rev1 (42) that catalyze error-free synthesis via the preferential incorporation of dCTP opposite the lesion. Although pol κ does not incorporate opposite O^6-MeG, it does participate in the elongation of O^6-MeG during error-free DNA synthesis (43). The dichotomy in polymerase function during error-prone versus

error-free synthesis has an important impact on the cellular maintenance of genomic integrity, especially in the context of current models accounting for translesion DNA synthesis. There are two contemporary models describing how DNA polymerase activity is coordinated during the by-pass of certain DNA lesions. These models, outlined in Figure 9, are based primarily on genetic and biochemical data for the replication of large, bulky DNA lesions such as thymine dimers (44–47). In one model, a replicative DNA polymerase incorporates a nucleotide opposite the lesion while extension is catalyzed by a specialized polymerase such as pol ζ. The second model differs in that the replicative polymerase does not incorporate opposite the lesion. Instead, a specialized polymerase such as pol η is recruited to correctly incorporate two dAMPs opposite the 3′ and 5′-thymine of the thymine dimer. Although this initial specialized DNA polymerase may extend beyond the lesion, an "extender" polymerase is typically invoked for efficient elongation. In both models, chromosomal replication is re-initiated by the re-binding of the replicative polymerase. While it is clear that the activity of specialized DNA polymerases is required to by-pass bulky lesions, the data provided here argues that this complex mechanism is not necessary when smaller, miscoding DNA lesions such as O^6-MeG are encountered. This is evident as O^6-MeG can be efficiently by-passed by the high-fidelity bacteriophage T4 DNA polymerase. As such, specialized DNA polymerases would not be not be needed to maintain the continuity of DNA replication during the by-pass of miscoding DNA lesions. However, the ability of specialized DNA polymerases to perform error-free DNA synthesis on these lesions may be essential to maintain genomic integrity. Further studies are clearly needed to deconvolute the mechanisms of lesion by-pass, especially considering that eukaryotes possess at least 15 different DNA polymerases (48), the majority of which replicate different forms of DNA damage with varying degrees of efficiency and fidelity.

Although lapses in exonuclease proofreading allow for elongation of the pro-mutagenic T:O^6-MeG mispair, it does prevent elongation of mispairs involving non-natural nucleotides such as P-nucleotide and Zebularine when paired opposite O^6-MeG. The results using Zebularine are particular striking as exonuclease proofreading rapidly and completely removes the incorporated non-natural nucleotide to make extension essentially impossible. Based on this, it is surprising that 4-MePoTP is extended almost as effectively as the natural nucleotide, dTTP, when paired opposite O^6-MeG even in the presence of vigorous exonuclease proofreading. Although the molecular mechanism accounting for this phenomenon is not clearly understood at this time, these data illustrate how pro-mutagenic consequences of a specific DNA lesion can be influenced by defective communication between polymerase and exonuclease active sites. In this case, communication between the polymerization and exonuclease domains of the phage polymerase appears to be regulated by a "rheostat" mechanism rather than a simple "on-off" switch. In this regard, the magnitude of exonuclease activity is controlled by a gradient in which structural features associated with the shape and geometry of a base pair are perturbed. Differences in base angles can be tolerated as long as the interglycosyl distance stays does not exceed a defined boundary of ~10.5Å. The details accounting for exonuclease activation are currently being explored by measuring the degradation of mispairs that differ with respect to interglycosyl distances and base angles.

Finally, these data also highlight the necessity of critically evaluating exonuclease proofreading activity in conjunction with polymerase activity to accurately define the pro-mutagenic potential of a DNA lesion. The use of mutant DNA polymerases that are deficient in exonuclease proofreading can avoid technical complications associated with studying the mechanism for nucleotide incorporation opposite various DNA lesions. However, results generated from such studies may show a bias that does not accurately reflect in vivo conditions. Hence, caution should be used when attempting to interpret the results of studies

examining replicative fidelity when using mutant DNA polymerases lacking exonuclease proofreading activity.

Materials and Methods

Materials

[γ-^{32}P]ATP was purchased from Perkin-Elmer. Unlabelled dNTPs (ultrapure) and were obtained from Pharmacia. $MgCl_2$, $Mg(OAc)_2$, and all buffers were from Sigma. All other materials were obtained from commercial sources and were of the highest available quality. The sequences of DNA substrates used in this study are provided in Figure 1B. Oligonucleotides, including those containing O^6-MeG, were obtained from Operon Technologies (Alameda, CA) and Sigma-Genosys (The Woodlands, TX). Single-stranded and duplex DNA were purified and quantified as previously described (18). Both wild-type and exonuclease-deficient D129A T4 DNA polymerase (Asp-219 to Ala mutation) were purified to homogeneity and quantified as previously described (49).

Methods

DNA was labeled by one of two methods. In the first protocol, duplex DNA was reacted with γ-^{32}P-ATP and polynucleotide kinase at 37°C for 30 minutes, heated at 65°C for 10 minutes, and then slowly cooled to 25°C. In the second protocol, single-stranded 13-mer DNA was first reacted with γ-^{32}P-ATP and polynucleotide kinase at 37° C for 30 minutes. After heating the sample at 65°C for 10 minutes to thermally inactivate polynucleotide kinase, an equimolar amount of 20-mer template DNA was added. After an additional 10 minutes at 65°C, the reaction was slowly cooled to 25°C and used in subsequent assays.

The assay buffer used in all kinetic studies consists of 25 mM Tris-OAc (pH 7.5), 150 mM KOAc, and 10 mM 2-mercaptoethanol. All assays, including rapid quench experiments using the instrument described by Johnson (24), were performed at 25°C. Polymerization reactions were monitored by analysis of the products on 20% sequencing gels as described by Mizrahi *et al.* (50). Gel images were obtained with a Packard PhosphorImager. Product formation was quantified by dividing the amount of ^{32}P-labelled extended by the total amount of ^{32}P-labelled (extended and non-extended primer). This provides a ratio in product formation which is then corrected for background using the same ratio measured in the absence of polymerase (zero point). Corrected ratios are then multiplied by the concentration of primer/template used in each assay to yield total product. All concentrations are listed as final solution concentrations.

Single Turnover Nucleotide Incorporation Assays—gp43 exo (1 μM) was incubated with 250 nM DNA (13/20G-mer or 13/20MeG-mer) in assay buffer containing EDTA (100 μM) and mixed with variable dNTP concentrations (0.005–5 mM) and 10 mM MgAcetate. The reactions were quenched with 500 mM EDTA at variable times (0.005–60 sec) and analyzed as described above. Data obtained for single turnover DNA polymerization assays were fit to equation 1.

$$y=A(1-e^{-kt})+C \quad (1)$$

where A is the burst amplitude, k is the first order rate constant, t is time, and C is a defined constant. Data for the dependency of k_{obs} as a function of dNTP were fit to the Michaelis-Menten equation (equation 2) to obtain values of k_{pol}, K_d for dNTP, and k_{pol}/K_d.

$$k_{obs}=k_{pol}[dNTP]/K_d+[dNTP] \quad (2)$$

where k_{obs} is the observed first-order rate constant, k_{pol} is the maximal rate constant of DNA polymerization, K_d is the kinetic dissociation constant for dNTP, and dNTP is the concentration of nucleotide substrate.

Kinetics of Extension Beyond a Mispair—Extension beyond the O^6-MeG lesion was performed under single turnover conditions using either wild type gp43 or gp43 exo . In these experiments, the rate constant for extending beyond O^6-MeG were measured in which 1 μM gp43exo or gp43 exo^+ was mixed with 250 nM DNA, 10 mM MgAcetate, and 250 μM dCTP or 250 μM dTTP. An aliquot of the reaction was quenched with 200 mM EDTA to insure incorporation opposite the lesion. 25 μM dGTP was then added to initiate extension beyond the potentially pre-mutagenic base pair. The reactions were quenched with 200 mM EDTA at variable times (5–180 sec) and analyzed as described above. Identical reactions were performed to measure elongation beyond unmodified guanine.

Supplementary Material

Refer to Web version on PubMed Central for supplementary material.

Acknowledgments

This work was supported by National Institutes of Health Grant (CA118408) to AJB. AIR was a PREP scholar supported by funding from the National Institutes of Health (GM075207).

Abbreviations

gp43 exo^-	exonuclease-deficient T4 DNA polymerase
gp43 exo^+	wild-type T4 DNA polymerase
O^6-MeG	O^6-methylguanine
EDTA	ethylenediaminetetraacetate sodium salt
TBE	Tris-HCl/borate/EDTA
dNTP	deoxynucleoside triphosphate
A	adenine
C	cytidine
G	guanine
T	thymine
dAMP	adenosine-2′-deoxyriboside monophosphate
dCMP	cytosine-2′-deoxyriboside monophosphate
dGMP	guanine-2′-deoxyriboside monophosphate
dTMP	thymine-2′-deoxyriboside monophosphate
dATP	adenosine-2′-deoxyriboside triphosphate
dCTP	cytosine-2′-deoxyriboside triphosphate
dGTP	guanine-2′-deoxyriboside triphosphate

dTTP	thymine-2′-deoxyriboside monophosphate, P-nucleotide, 2R,3R,5R-3-hydroxy-5-(7-oxo-7,8-dihydro-3H-pyrimido[4,5-c][1,2]oxazin-6(4H)-yl)tetrahydrofuran-2-yl)methyl deoxyriboside triphosphate
4-MePoTP	4-methyl-pyrimidone-2′-deoxynucleoside triphosphate
Zebularine	2-pyrimidone-2′-deoxynucleoside triphosphate

References

1. Kunkel TA, Bebenek K. DNA replication fidelity. Annu Rev Biochem. 2000; 69:497–529. [PubMed: 10966467]
2. Grevatt PC, Solomon JJ, Bhanot OS. *In vitro* mispairing specificity of O2-ethylthymidine. Biochemistry. 1992; 31:4181–4188. [PubMed: 1567865]
3. Marcelino LA, Andre PC, Khrapko K, Coller HA, Griffith J, Thilly WG. Chemically induced mutations in mitochondrial DNA of human cells: mutational spectrum of N-methyl-N′-nitro-N-nitrosoguanidine. Cancer Res. 1998; 58:2857–2862. [PubMed: 9661902]
4. Yan SF, Wu M, Geacintov NE, Broyde S. Altering DNA polymerase incorporation fidelity by distorting the dNTP binding pocket with a bulky carcinogen-damaged template. Biochemistry. 2004; 43:7750–7765. [PubMed: 15196018]
5. Monti P, Traverso I, Casolari L, Menichini P, Inga A, Ottaggio L, Russo D, Iyer P, Gold B, Fronza G. Mutagenicity of N3-methyladenine: a multi-translesion polymerase affair. Mutat Res. 2010; 683:50–56. [PubMed: 19874831]
6. Li HY, Wang SM, Liu HM, Bu SS, Li J, Han D, Zhang MZ, Wu GY. Separation and identification of purine nucleosides in the urine of patients with malignant cancer by reverse phase liquid chromatography/electrospray tandem mass spectrometry. J Mass Spectrom. 2009; 44:641–651. [PubMed: 19142897]
7. Margison GP, Santibáñez Koref MF, Povey AC. Mechanisms of carcinogenicity/chemotherapy by O6-methylguanine. Mutagenesis. 2002; 17:483–487. [PubMed: 12435845]
8. Quiros S, Roos WP, Kaina B. Processing of O6-methylguanine into DNA double-strand breaks requires two rounds of replication whereas apoptosis is also induced in subsequent cell cycles. Cell Cycle. 2010; 9:168–178. [PubMed: 20016283]
9. Casorelli I, Russo MT, Bignami M. Role of mismatch repair and MGMT in response to anticancer therapies. Anticancer Agents Med Chem. 2008; 8:368–380. [PubMed: 18473722]
10. Mishina Y, Duguid EM, He C. Direct reversal of DNA alkylation damage. Chem Rev. 2006; 106:215–232. [PubMed: 16464003]
11. Marchesi F, Turriziani M, Tortorelli G, Avvisati G, Torino F, De Vecchis L. Triazene compounds: mechanism of action and related DNA repair systems. Pharmacol Res. 2007; 56:275–287. [PubMed: 17897837]
12. Spratt TE, Levy DE. Structure of the hydrogen bonding complex of O6-methylguanine with cytosine and thymine during DNA replication. Nucleic Acids Res. 1997; 25:3354–3361. [PubMed: 9241252]
13. Woodside AM, Guengerich FP. Effect of the O6 substituent on misincorporation kinetics catalyzed by DNA polymerases at O(6)-methylguanine and O(6)-benzylguanine. Biochemistry. 2002; 41:1027–1038. [PubMed: 11790127]
14. Perrino FW, Blans P, Harvey S, Gelhaus SL, McGrath C, Akman SA, Jenkins GS, LaCourse WR, Fishbein JC. The N2-ethylguanine and the O6-ethyl- and O6-methylguanine lesions in DNA: contrasting responses from the “bypass” DNA polymerase eta and the replicative DNA polymerase alpha. Chem Res Toxicol. 2003; 16:1616–1623. [PubMed: 14680376]
15. Warren JJ, Forsberg LJ, Beese LS. The structural basis for the mutagenicity of O(6)-methylguanine lesions. Proc Natl Acad Sci USA. 2006; 103:19701–19706. [PubMed: 17179038]
16. Kunkel TA, Loeb LA, Goodman MF. On the fidelity of DNA replication. The accuracy of T4 DNA polymerases in copying phi X174 DNA *in vitro*. J Biol Chem. 1984; 259:1539–1545. [PubMed: 6229537]

17. Santos ME, Drake JW. Rates of spontaneous mutation in bacteriophage T4 are independent of host fidelity determinants. Genetics. 1994; 138:553–564. [PubMed: 7851754]
18. Capson TL, Peliska JA, Kaboord BF, Frey MW, Lively C, Dahlberg M, Benkovic SJ. Kinetic characterization of the polymerase and exonuclease activities of the gene 43 protein of bacteriophage T4. Biochemistry. 1992; 31:10984–10994. [PubMed: 1332748]
19. Spicer EK, Rush J, Fung C, Reha-Krantz LJ, Karam JD, Konigsberg WH. Primary structure of T4 DNA polymerase. Evolutionary relatedness to eucaryotic and other procaryotic DNA polymerases. J Biol Chem. 1988; 263:7478–7486. [PubMed: 3286635]
20. Benkovic SJ, Cameron CE. Kinetic analysis of nucleotide incorporation and misincorporation by Klenow fragment of *Escherichia coli* DNA polymerase I. Methods Enzymol. 1995; 262:257–269. [PubMed: 8594352]
21. Joyce CM, Benkovic SJ. DNA polymerase fidelity: kinetics, structure, and checkpoints. Biochemistry. 2004; 43:14317–14324. [PubMed: 15533035]
22. Berdis AJ. Mechanisms of DNA polymerases. Chem Rev. 2009; 109:2862–2879. [PubMed: 19489544]
23. Johnson KA. The kinetic and chemical mechanism of high-fidelity DNA polymerases. Biochim Biophys Acta. 2010; 1804:1041–1048. [PubMed: 20079883]
24. Johnson KA. Rapid quench kinetic analysis of polymerases, adenosinetriphosphatases, and enzyme intermediates. Methods Enzymol. 1995; 249:38–61. [PubMed: 7791620]
25. Berdis AJ. Dynamics of translesion DNA synthesis catalyzed by the bacteriophage T4 exonuclease-deficient DNA polymerase. Biochemistry. 2001; 40:7180–7191. [PubMed: 11401565]
26. Furge LL, Guengerich FP. Analysis of nucleotide insertion and extension at 8-oxo-7,8-dihydroguanine by replicative T7 polymerase exo- and human immunodeficiency virus-1 reverse transcriptase using steady-state and pre-steady-state kinetics. Biochemistry. 1997; 36:6475–6487. [PubMed: 9174365]
27. Einolf HJ, Guengerich FP. Kinetic analysis of nucleotide incorporation by mammalian DNA polymerase delta. J Biol Chem. 2000; 275:16316–16322. [PubMed: 10748013]
28. Choi JY, Chowdhury G, Zang H, Angel KC, Vu CC, Peterson LA, Guengerich FP. Translesion synthesis across O6-alkylguanine DNA adducts by recombinant human DNA polymerases. J Biol Chem. 2006; 281:38244–38256. [PubMed: 17050527]
29. Frey MW, Nossal NG, Capson TL, Benkovic SJ. Construction and Characterization of a bacteriophage T4 DNA polymerase deficient in 3′→5′ exonuclease activity. Proc Natl Acad Sci USA. 1989; 90:2579–2583. [PubMed: 8464864]
30. Wong I, Patel SS, Johnson KA. An induced-fit kinetic mechanism for DNA replication fidelity: direct measurement by single-turnover kinetics. Biochemistry. 1991; 30:526–537. [PubMed: 1846299]
31. Tsai YC, Johnson KA. A new paradigm for DNA polymerase specificity. Biochemistry. 2006; 45:9675–9687. [PubMed: 16893169]
32. Matsuda S, Romesberg FE. Optimization of interstrand hydrophobic packing interactions within unnatural DNA base pairs. J Am Chem Soc. 2004; 126:14419–14427. [PubMed: 15521761]
33. Leconte AM, Hwang GT, Matsuda S, Capek P, Hari Y, Romesberg FE. Discovery, characterization, and optimization of an unnatural base pair for expansion of the genetic alphabet. J Am Chem Soc. 2008; 130:2336–2343. [PubMed: 18217762]
34. Zhang X, Motea E, Lee I, Berdis AJ. Replication of a universal nucleobase provides unique insight into the role of entropy during DNA polymerization and pyrophosphorolysis. Biochemistry. 2010; 49:3009–3023. [PubMed: 20187654]
35. Motea EA, Lee I, Berdis AJ. Quantifying the energetic contributions of desolvation and {pi}-electron density during translesion DNA synthesis. Nucleic Acids Res. 2011; 39:1623–1637. [PubMed: 20952399]
36. Moran S, Ren RX, Kool ET. A thymidine triphosphate shape analog lacking Watson-Crick pairing ability is replicated with high sequence selectivity. Proc Natl Acad Sci USA. 1997; 94:10506–10511. [PubMed: 9380669]

37. Kool ET. Active site tightness and substrate fit in DNA replication. Annu Rev Biochem. 2002; 71:191–219. [PubMed: 12045095]

38. Patel DJ, Shapiro L, Kozlowski SA, Gaffney BL, Jones RA. Structural studies of the O6meG. C interaction in the d(C-G-C-G-A-A-T-T-C-O6meG-C-G) duplex. Biochemistry. 1986; 25:1027–1036. [PubMed: 3964658]

39. Leonard GA, Thomson J, Watson WP, Brown T. High-resolution structure of a mutagenic lesion in DNA. Proc Natl Acad Sci USA. 1990; 87:9573–9576. [PubMed: 2263612]

40. Eoff RL, Irimia A, Egli M, Guengerich FP. Sulfolobus solfataricus DNA polymerase Dpo4 is partially inhibited by “wobble” pairing between O6-methylguanine and cytosine, but accurate bypass is preferred. J Biol Chem. 2006; 282:1456–1467. [PubMed: 17105728]

41. Haracska L, Prakash S, Prakash L. Replication past O(6)-methylguanine by yeast and human DNA polymerase eta. Mol Cell Biol. 2000; 20:8001–8007. [PubMed: 11027270]

42. Haracska L, Prakash S, Prakash L. Yeast Rev1 protein is a G template-specific DNA polymerase. J Biol Chem. 2002; 277:15546–15551. [PubMed: 11850424]

43. Haracska L, Prakash L, Prakash S. Role of human DNA polymerase kappa as an extender in translesion synthesis. Proc Natl Acad Sci USA. 2002; 99:16000–16005. [PubMed: 12444249]

44. Gratchev A, Strein P, Utikal J, Sergij G. Molecular genetics of *Xeroderma pigmentosum* variant. Exp Dermatol. 2003; 12:529–536. [PubMed: 14705792]

45. Wang Y, Woodgate R, McManus TP, Mead S, McCormick JJ, Maher VM. Evidence that in xeroderma pigmentosum variant cells, which lack DNA polymerase eta, DNA polymerase iota causes the very high frequency and unique spectrum of UV-induced mutations. Cancer Res. 2007; 67:3018–3026. [PubMed: 17409408]

46. Stary A, Sarasin A. Molecular mechanisms of UV-induced mutations as revealed by the study of DNA polymerase eta in human cells. Res Microbiol. 2002; 153:441–445. [PubMed: 12405351]

47. Nelson JR, Lawrence CW, Hinkle DC. Thymine-thymine dimer bypass by yeast DNA polymerase zeta. Science. 1996; 272:1646–1649. [PubMed: 8658138]

48. Goodman MF, Tippin B. The expanding polymerase universe. Nat Rev Mol Cell Biol. 2000; 1:101–109. [PubMed: 11253362]

49. Rush J, Konigsberg WH. Rapid purification of overexpressed T4 DNA polymerase. Prep Biochem. 1989; 19:329–340. [PubMed: 2622873]

50. Mizrahi V, Benkovic P, Benkovic SJ. Mechanism of DNA polymerase I: exonuclease/polymerase activity switch and DNA sequence dependence of pyrophosphorolysis and misincorporation reactions. Proc Natl Acad Sci USA. 1986; 83:5769–5773. [PubMed: 3016719]

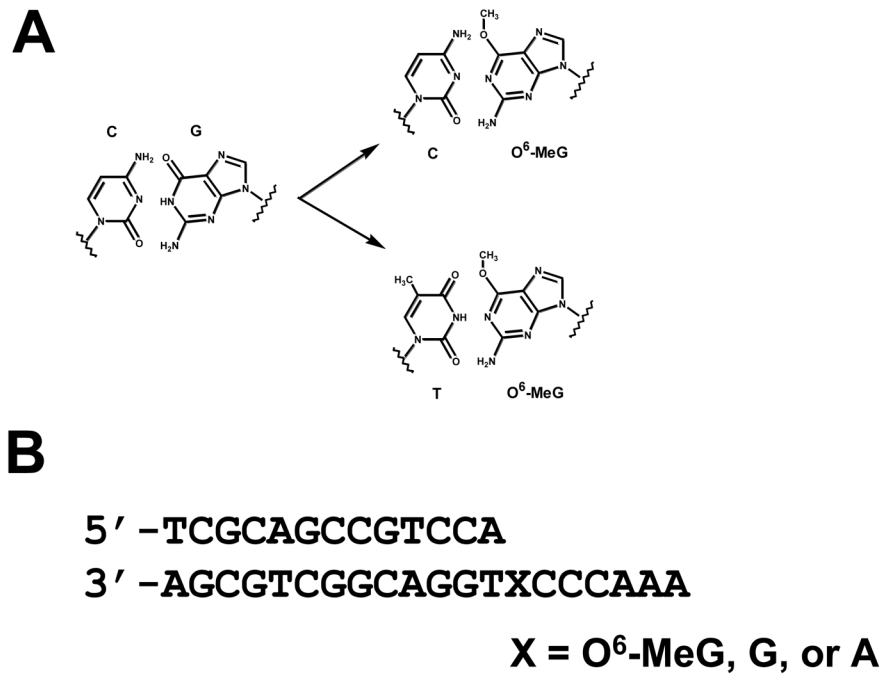

Figure 1.
(A) Structures for C:O^6-MeG and T:O^6-MeG based upon Watson-Crick hydrogen bonding capabilities. (B) DNA substrates used for all kinetic analyses. MeG denotes O^6-methylguanine.

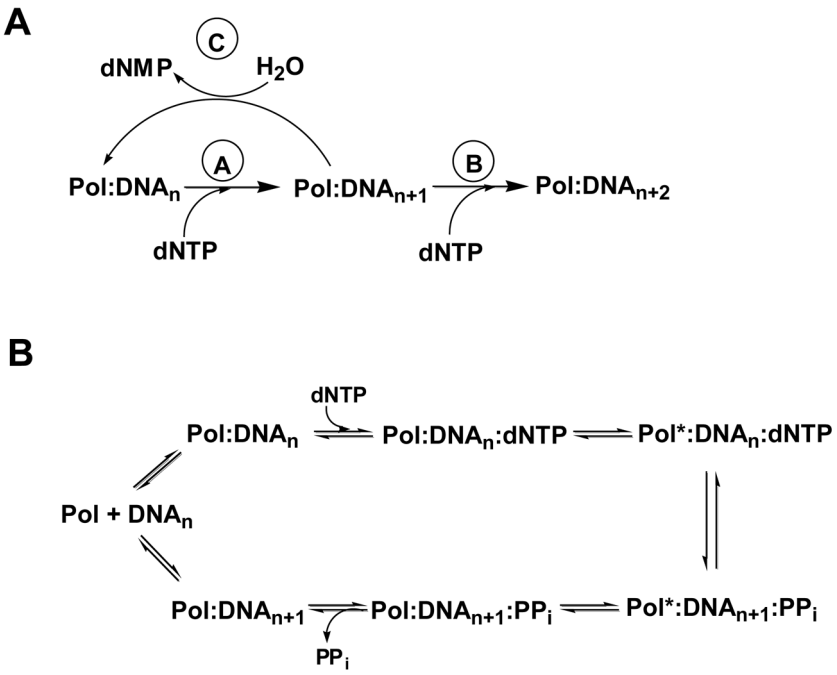

Figure 2.
(A) Interplay of polymerization, extension, and exonuclease proofreading in the maintenance of genomic fidelity during DNA replication. (B) Minimal kinetic mechanism for DNA polymerization. Step 1 represents dNTP binding to the polymerase:nucleic acid complex. Step 2 represents the conformational change prior to phosphoryl transfer. Step 3 represents phosphoryl transfer. Step 4 represents the conformational change after phosphoryl transfer. Step 5 represents the release of the first product, pyrophosphate. Step 6 collectively represents translocation of the enzyme to the next insertion position and binding of the next correct dNTP. Abbreviations are as follows: Pol = bacteriophage T4 DNA polymerase, DNA_n= DNA substrate, Pol' = conformational change in DNA polymer ase, PP_i = inorganic pyrophosphate, and DNA_{n+1} = DNA product (DNA extended by one nucleobase).

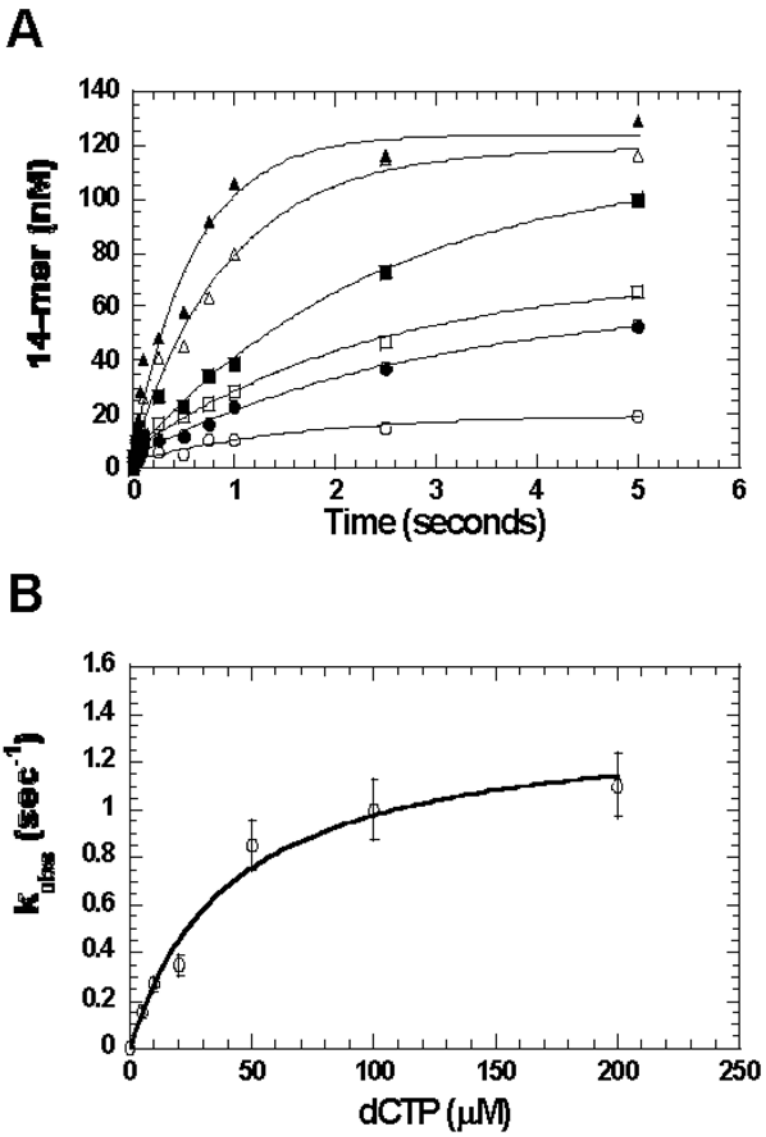

Figure 3.
(A) gp43 exo (1000 nM) and 5′-labeled 13/20MeG-mer (250 nM) were preincubated, mixed with 10 mM Mg^{2+} and variable concentrations of dCTP to initiate the reaction, and quenched with 500 mM EDTA at variable times (0.005–0.25 sec). The incorporation of dCTP was analyzed by denaturing gel electrophoresis. dCTP concentrations were 5 μM (O), 10 μM (●), 25 μM (❸), 50 μM (■), 100 μM (△), and 200 μM (▲). The solid lines represent the fit of the data to a single exponential. (B) The plot of observed rate constants for dCTP incorporation (O) versus dCTP concentration are hyperbolic. A fit of the data to the Michaelis-Menten equation was used to provide a k_{pol} of 1.5 +/− 0.2 sec^{-1} and a K_d of 48+/− 16 μM.

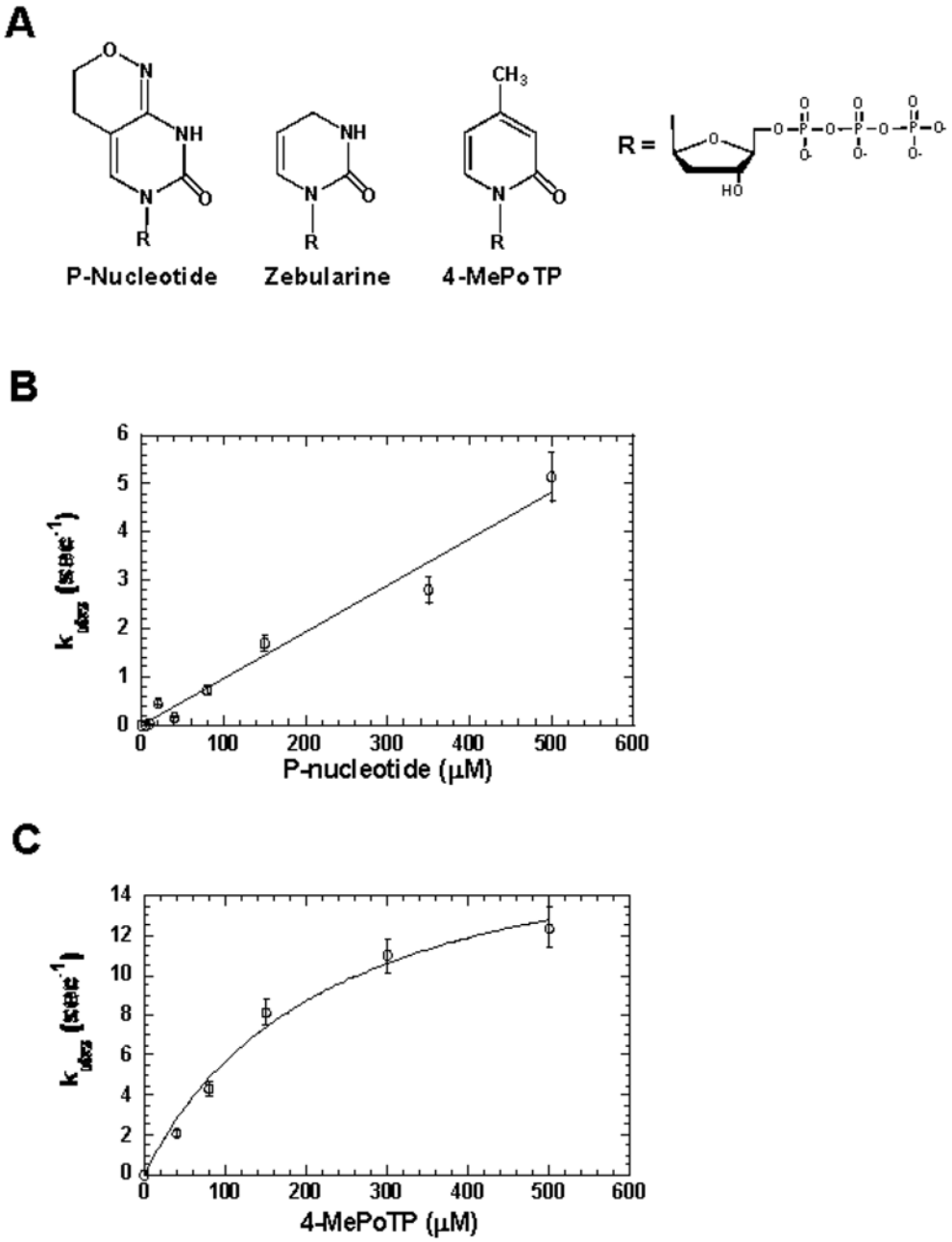

Figure 4.
(A) Structures of the three non-natural nucleotides used in this study (P-nucleotide, Zebularine, and 4-MePoTP). (B) Plot of the observed rate constant for incorporating P-nucleotide opposite O^6-MeG (O) as a function of concentration of P-nucleotide concentration. Under the concentrations tested, the plot is linear and provides a value of 21,000 +/−8,000 $M^{-1}sec^{-1}$ for the catalytic efficiency for incorporating P-nucleotide opposite O^6-MeG. (C) The plot of observed rate constants for 4-MePoTP incorporation (O) versus nucleotide concentration. A fit of the data to the Michaelis-Menten equation was used to provide a k_{pol} of 18 +/− 1.2 sec^{-1} and a K_d of 202 +/− 30 μM for 4-MePoTP opposite O^6-MeG.

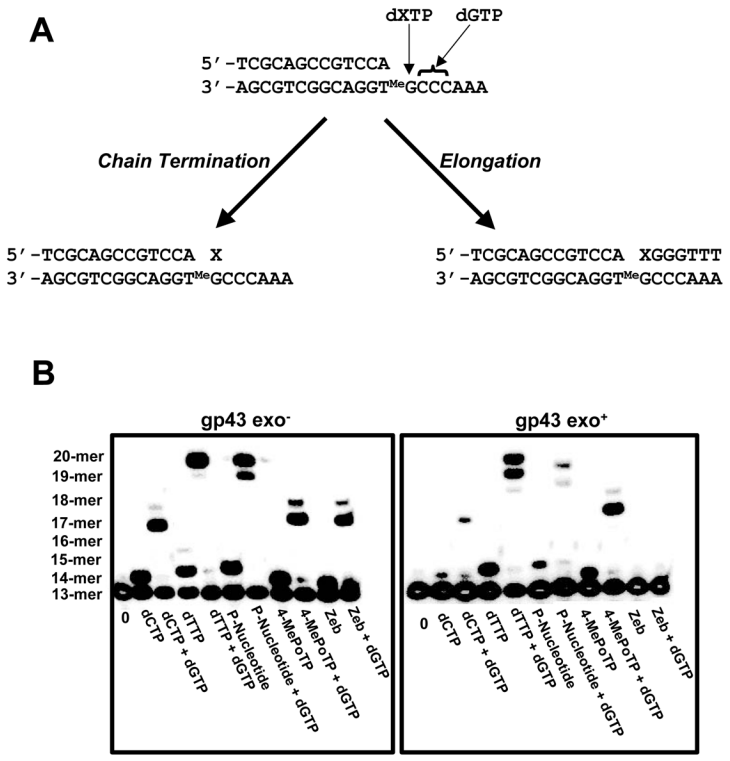

Figure 5.
(A) Experimental protocol used to monitor extension beyond correct or mismatched base pairs. See text for details. (B) Extension of natural and non-natural mispairs containing O^6-MeG by gp43 exo . Experiments were performed by adding a fixed concentration of natural (dCTP or dTTP) or non-natural nucleotide (P-nucleotide, Zebularine, or 4-MePoTP) to a preincubated solution of 1 μM gp43 exo$^-$ and 500 nM 13/20MeG-mer. An aliquot of the reaction was quenched with 200 mM EDTA. After this time, 500 μM dGTP was added to initiate elongation beyond the mispair. An aliquot of the reaction was quenched with 200 mM EDTA after 1 minute (natural dNTPs) or 5 minutes (non-natural nucleotides). Reaction products are separated on a 20% denaturing polyacrylamide gel. The lane demarcated as "0" depicts unextended primer/template. All other lanes are labeled according to the nucleotides added. (C) Extension of various mispairs by gp exo$^+$. All assays were performed using similar protocols described above using gp43 exo .

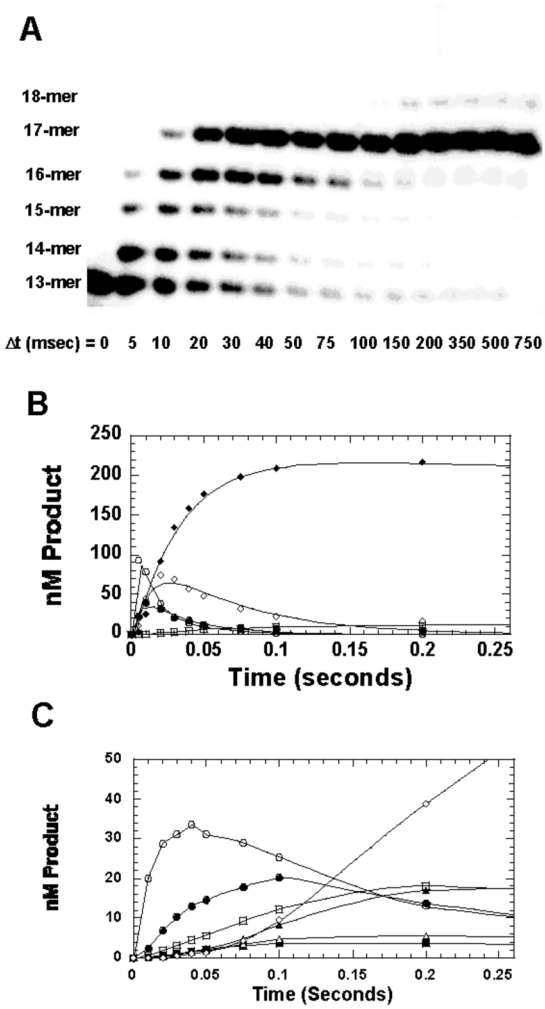

Figure 6.
(A) Kinetics of extension beyond a C:G base pair. 1 μM gp43 exo was preincubated with 500 nM 13/20G-mer, mixed with 10 mM Mg^{2+} and 25 μM dCTP/25 μM dGTP to initiate the reaction, and quenched with 500 mM EDTA at variable times (0.005–0.15 sec). Reaction products are separated on a 20% denaturing polyacrylamide gel. Lanes demarcated as "0" depict unextended primer/template only. (B) The data obtained from gel electrophoresis show the sequential accumulation of products. Product formation is denoted as follows: ○ = 14-mer, ● = 15-mer, ◇ = 16-mer, ■ = 17-mer, and ❸ = 18-mer. Fits of the data in product formation were generated using the rate constants denoted in Table 2 which were obtained through computer simulation of the data. (C) Time course for extension beyond a T:O^6-MeG mismatch catalyzed by gp43 exo^-. Product formation is denoted as follows: ○ = 14-mer, ● = 15-mer, ❸ = 16-mer, ■ = 17-mer, △ = 18-mer, ▲ = 19-mer, and ◇ = 20-mer. The curves for product formation were generated using the rate constants denoted in Table 2 obtained through computer simulation (20) of the data.

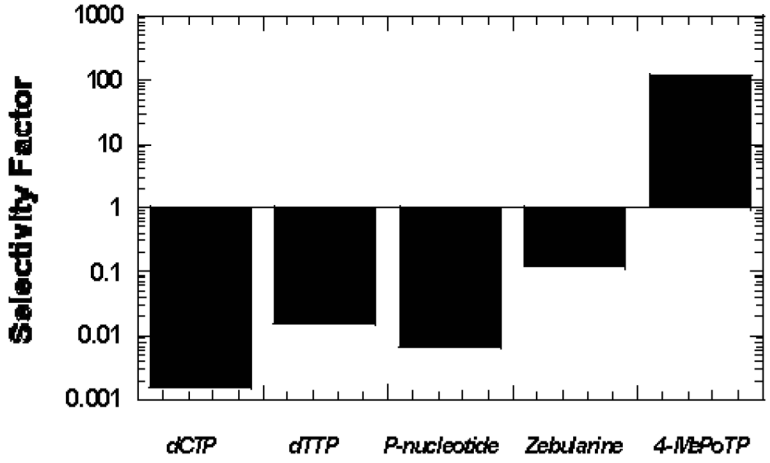

Figure 7.
Representation of the selectivity factor for natural and non-natural nucleotides for incorporation opposite O^6-methylguanine. Selectivity factor is defined as $(k_{pol}/K_d)_{O6\text{-}MeG}/(k_{pol}/K_d)_{G\ or\ A.}$ As illustrated, 4-MePoTP displays a selectivity factor of ~100 for incorporation opposite O^6-methylguanine whereas other nucleotides tested show selectivity factors of less than 1.

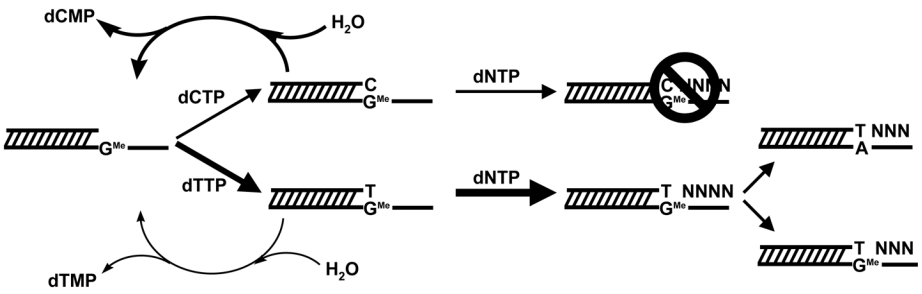

Figure 8.
Model for the coordination of polymerization and exonuclease activity during the misreplication of the miscoding DNA lesion, O^6-methylguanine. See text for details.

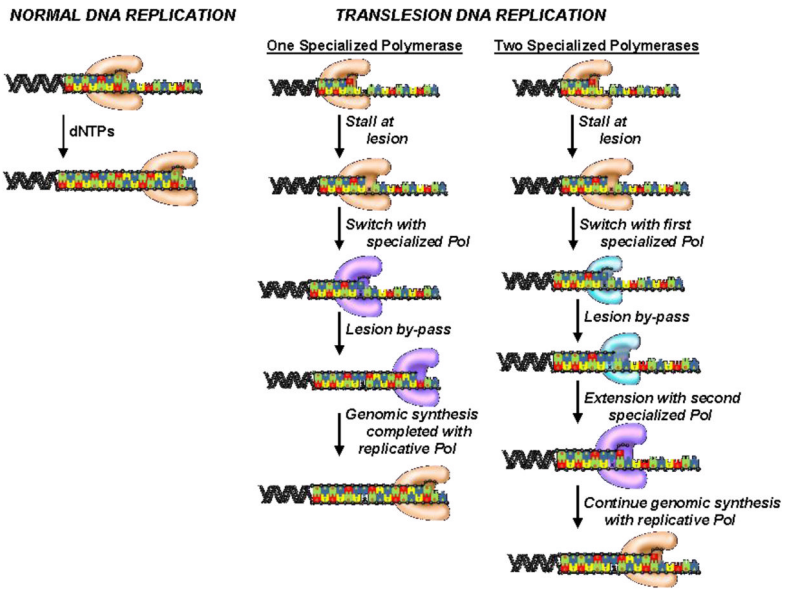

Figure 9.
Models for correct and translesion DNA synthesis involving the coordinated activities of replicative and specialized DNA polymerases. See text for details.

Table 1

Summary of kinetic parameters for the incorporation of natural and non-natural nucleotides O^6-methylguanine, guanine, or adenine catalyzed by the bacteriophage T4 DNA polymerase.[a]

Substrate	dNTP	k_{pol} (sec^{-1})	K_d (μM)	k_{pol}/K_d ($M^{-1}sec^{-1}$)
13/20MeG	dCTP	1.5 ± 0 2	48 ± 16	$(3.1 \pm 0.5)*10^4$
13/20MeG	dTTP	114 ± 20	760 ± 230	$(1.5 \pm 0.4)*10^5$
13/20MeG	P-Nucleotide	>10	>500	$(2\ 1+/-0.8)*10^4$ [b]
13/20MeG	Zebularine	0 11 ± 0.03	660 ± 100	$(1.7 \pm 0.5)*10^2$
13/20MeG	4-MePoTP	18 ± 1 2	202 ± 20	$(8.9 \pm 0.4)*10^4$
13/20G	dCTP	118 ± 7	5.9 ± 1 1	$(2.0 \pm 0.1)*10^7$
13/20G	dTTP	0.019 ± 0.002	16 ± 4	$(1.2 \pm 0.1)*10^3$
13/20G	dATP	0.020 ± 0.002	160 ± 50	$(1.3 \pm 0.4)*10^2$
13/20G	P-Nucleotide	45 ± 6	72 ± 20	$(6.3 \pm 0.6)*10^5$
13/20G	Zebularine	<0.5	>350	$(1.4 \pm 0.5)*10^3$ [b]
13/20G	4-MePoTP	0.40 ± 0.05	550 ± 110	$(7.3 \pm 1.5)*10^2$
13/20A	dCTP	0 12 ± 0.01	350 ± 40	$(3.4 \pm 0.5)*10^2$
13/20A	P-Nucleotide	77 ± 8	27 ± 8	$(2.9 \pm 0.4)*10^6$
13/20A	4-MePoTP	ND [c]	ND	ND
13/20A	Zebularine	>0.1	>500	$(2.0 \pm 0.6)*10^2$ [b]

[a] gp43 exo (1 μM) was incubated with 250 nM DNA and mixed with variable concentrations of dNTP (0.005–5 mM) and 10 mM MgAcetate.

[b] Accurate k_{pol}/K_d values were obtained from the slope of the line form the plot of rate constant versus dNTP concentration.

[c] Kinetic parameters were not determined as product was not detected even at substrate concentrations greater than 350 μM.

Table 2

Kinetic rate constants for incorporation opposite and beyond G or O^6-MeG[a].

Position	13/20G Correct	13/20G Incorrect [c]	13/20MeG dCTP, dGTP	13/20MeG dTTP, dGTP [c]
13->14 (n+1)	100 sec^{-1}	0.019 sec^{-1} [b]	1.5 sec^{-1} [b]	20 sec^{-1}
14->15 (n+2)	100 sec^{-1}	2.7 sec^{-1}	2.5 sec^{-1}	50 sec^{-1}
15->16 (n+3)	50 sec^{-1}	0.3 sec^{-1}	150 sec^{-1}	50 sec^{-1}
16->17 (n+4)	100 sec^{-1}	20 sec^{-1}	20 sec^{-1}	50 sec^{-1}

[a] Time courses for extending beyond correct or incorrectly paired primer/templates were performed using 1 μM gp43 exo , 250 nM DNA, 10 mM Mg^{2+}, and the following dNTP concentrations: 25 μM dCTP and 25 μM dGTP with 13/20G-mer; 25 μM dGTP with 14T/20G-mer and 14C/20MeG-mer; and 250 μM dTTP and 25 μM dGTP with 13/20MeG-mer. Rate constants were obtained using computer simulation to fit the time courses in product formation. See text for further discussions.

[b] The rate constant provided here reflects the k_{pol} value measured previously under single turnover conditions in the absence of dGTP.

[c] Products corresponding to 18-, 19-, and 20-mers are observed under these reaction conditions. For convenience, the rate constants corresponding to their formation are not provided.

Table 3

Correlation between the elongation kinetics of correct and mismatched base pairs with their calculated biophysical parameters.

Base pair	Extension by gp43 exo$^-$	Extension by gp43 exo$^+$	C1′ to C1′ (Å)[b]	∠A_1 (°)[c]	∠A_2 (°)[c]
T:A	++++[a]	++++	10.5	55.4	56 1
C:G	++++	++++	10.2	53.3	55.7
T:G	+++	−	10.4	40.1	69 9
A:G	−	−	12.5	52.0	53.0
C:O^6-MeG	+++	+	11.4	65.9	43.0
T:O^6-MeG	++++	+++	10.5	53.3	52 2
P-Nucl:O^6-MeG	++	+	11.2	43.4	64.7
Zeb:O^6-MeG	++	−	ND[d]	ND	ND
4-MePo:O^6-MeG	+++	+++	10.8	64.6	60.0

[a] The following scale was used to signify ranges in the rate constants for extending correct and mismatched DNA: ++++ = k_{ext} values ≥ 10 sec ^{1}, +++ = k_{ext} values ~1 sec ^{1}, ++ = k_{ext} values ~ 0.1 sec ^{1}, + = k_{ext} values ~ 0.01 sec ^{1}, and − indicates no extension.

[b] Interglycosyl distance refers to the shortest length between the C1′ of either ribosyl group in the base pair and loosely defines the geometry of helical DNA.

[c] Nucleobase angle refers to the angle between the C1 of ribose with the N9 of a purine or N1 of pyrimidine of a specific nucleobase.

[d] Not determined.